minerals

MDPI

Article

Effects of Sample Shapes and Thickness on Distribution of Temperature inside the Mineral Ilmenite Due to Microwave Heating

Mas Irfan P. Hidayat [1,*], Dian M. Felicia [1], Ferdiansyah I. Rafandi [2] and Affiani Machmudah [3]

[1] Department of Materials and Metallurgical Engineering-FTIRS, Institut Teknologi Sepuluh Nopember (ITS), Surabaya 60111, Indonesia; dian.mughni@gmail.com
[2] GUNTNER-TATA, Güntner-Tata Hűtőtechnika Kft, 2890 Tata, Hungary; iqbal.mamet@gmail.com
[3] School of Advance Technology and Multidisciplinary, Universitas Airlangga, Kampus C Jalan Mulyorejo, Surabaya 60115, Indonesia; affiani.machmudah@fst.unair.ac.id
* Correspondence: masirfan.ph@gmail.com or irfan@mat-eng.its.ac.id

Received: 21 March 2020; Accepted: 15 April 2020; Published: 23 April 2020

Abstract: The study of interaction between microwave radiation and minerals is gaining increasing interest in the field of minerals and material processing. Further studies are, however, still required to deepen the understanding of such microwave heating mechanisms in order to develop innovative techniques for mineral treatment using microwave heating. In this paper, effects of sample shapes and thickness on the distribution of temperature inside the mineral ilmenite ($FeTiO_3$) due to microwave heating were numerically studied using the finite element (FE) method. The analysis was carried out in such a way that the flux of microwave energy was converted into an equivalent amount of heat generation in the mineral through the Poynting theorem of conservation of energy for the electromagnetic field. In this study, as a first attempt, the cylinder and slab of ilmenite were modeled to be irradiated from top and bottom surfaces with the variation of cylinder and slab thicknesses. Temperature-dependent material properties of ilmenite were taken into account in the FE simulation. Corresponding boundary conditions were then applied accordingly to the cylinder and slab of ilmenite with comparable characteristic length. Numerical results showed that, in terms of temperature differences between locations having maximum and minimum temperatures, slab geometries tended to produce higher values in comparison to those of cylinder geometries with the thickness variation, while the profiles of temperature inside the ilmenite samples were similar for both geometries. For the same duration of microwave heating, the slab geometry, hence, induced greater non-uniformity of temperature inside the ilmenite. It was also observed that, for the ilmenite samples with thickness value greater than 1.5 cm, the hotspot locations were not in the center of the sample, but on the surface of sample. Moreover, from several thickness values considered in this study, the ilmenite sample with thickness value of 3 cm gave a good trade-off between the maximum temperature value attained and temperature differences inside the sample, for both geometries. Thus, the shape and thickness of ilmenite samples affect the effectiveness of microwave heating of ilmenite, in terms of maximum temperature attained, temperature differences, and uniformity of temperature.

Keywords: mineral processing; microwave heating; ilmenite ($FeTiO_3$); heat source; non-uniform temperature

1. Introduction

Microwave-assisted heating is extensively used in mineral and material processing. For material processing, microwave heating has several advantages including deep penetration, volumetric heating, and a controlled source of power [1–3]. As a result, the study of interactions between microwave

radiation and minerals gained increasing interest in recent years [4]. Despite the facts, this method could nonetheless generate non-uniform temperature distribution during the heating process, which is still a main challenge [5,6]. Further studies are, hence, required to deepen the understanding of such microwave heating mechanisms in order to develop innovative techniques for mineral treatment using microwave heating.

Among mineral resources, ilmenite ($FeTiO_3$) concentrates are important feeds for the production of titanium dioxide (TiO_2) pigments via a number of industrial processes. In Indonesia, placer deposits for ilmenite are estimated to amount of 40 million tons [7]. Magmatic deposits can yield ilmenite with a TiO_2 content of 35%–40% mass fraction, whereas placer deposits provide ilmenite of higher TiO_2 content [8]. Commonly, microwave heating is preferred in the industrial processes, as processes involved in the production stages can be highly energy-intensive and -consuming. For instance, extensive chemical alteration is needed to facilitate the preferential removal of iron from the ilmenite [9–11]. Details of such removal and enrichment processes can be found in Reference [9].

It is interesting to note that, while studies on microwave heating for mineral processing were intensively reported in literature [12–15], related numerical studies are nonetheless still limited. On the other hand, modeling of microwave heating of foods was the main concern so far in the literature [16–18]. This research work, hence, fills the gap concerning modeling and numerical simulations of microwave heating for mineral processing, particularly ilmenite. Readers are kindly referred to Reference [19] for details of the microwave heating mechanism, particularly in relationship with particle morphology and characteristics.

In this paper, the effects of sample shape and thickness on the distribution of temperature inside the mineral ilmenite ($FeTiO_3$) due to microwave heating were numerically studied using the finite element (FE) method (FEM). FEM was chosen as a numerical solver in this study due to its well-known robustness for heat transfer modeling. Moreover, FEM handles problems of unsteady volumetric heating in a straightforward manner such as that investigated here, where heat generation arising inside a sample due to microwave heating manifests itself as transient volumetric heating. This is in contrast to, for instance, the time-stepping boundary element (BE) scheme in handling transient problems, as the transient effect reveals itself as an additional volume integral, thus giving additional complexity in computation [20]. In this work, the analysis was carried out in such a way that the flux of microwave energy was converted into an equivalent amount of heat generation in the mineral through the Poynting theorem of conservation of energy for the electromagnetic field. In this study, as a first attempt, cylinders and slabs of ilmenite were modeled to be irradiated from top and bottom surfaces. Temperature-dependent material properties of ilmenite were taken into account in the simulation. Corresponding boundary conditions were then applied accordingly to the cylinder and slab of ilmenite with comparable characteristic length. Numerical results of transient temperature distribution inside the ilmenite with the variation of cylinder and slab heights are presented and discussed. The obtained temperature results are further corroborated with available data from practical microwave heating processes of ilmenite in the literature.

2. Materials and Methods

2.1. Formulation of Electromagnetic Wave and Energy

Figure 1 shows a schematic of microwave heating for cylinder object. A typical FE mesh employed is also shown in Figure 1. Using the assumptions of uniform plane waves and linear material constitutive laws to approximate the actual electric field in a system, the Maxwell equations may be simplified as follows [21–23]:

$$\vec{J} = \sigma' \vec{E} \tag{1}$$

$$\vec{D} = \varepsilon \vec{E} \tag{2}$$

$$\vec{B} = \mu \vec{H} \tag{3}$$

where $\vec{J}$ is the current density, $\vec{D}$ is the electric displacement, $\vec{B}$ is the magnetic induction, σ' is the electrical conductivity, ε is the permittivity, and μ is the magnetic permeability.

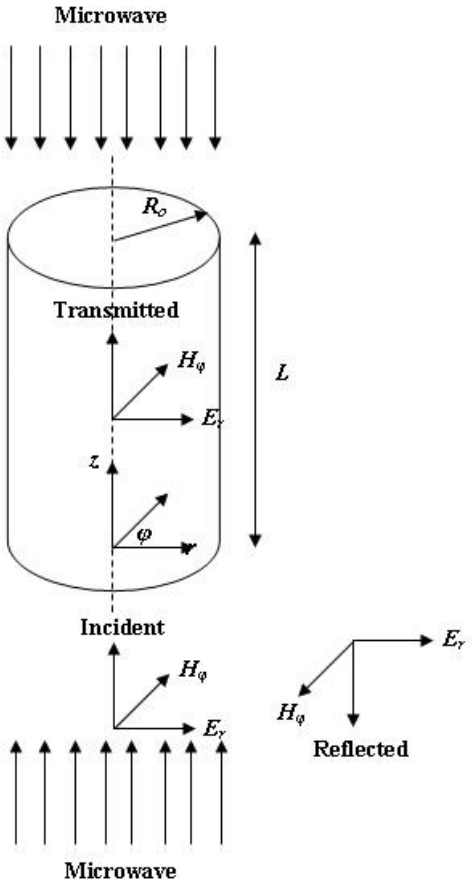

(**a**)

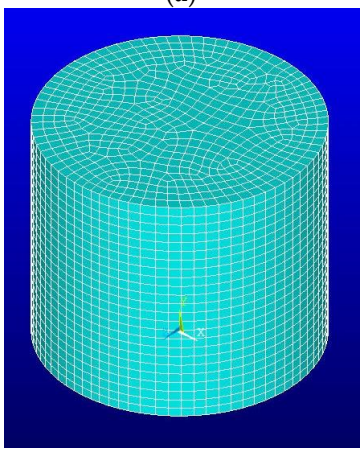

(**b**)

Figure 1. Schematic of microwave heating for cylinder object: (**a**) cylinder; (**b**) typical FE mesh for the cylinder object.

Following Reference [22,23], under the uniform plane wave assumption, the simplified equation for electric field can be further written as follows:

$$\frac{d^2E_r}{dz^2} + \chi^2 E_r = 0 \tag{4}$$

where χ is the propagation constant, and z is the axial direction. The constant may be expressed as $\chi = \sigma + i\beta$ with the following phase factor:

$$\sigma = \frac{2\pi f}{c}\sqrt{\frac{\kappa'\left(\sqrt{1+\tan^2\delta}+1\right)}{2}} \tag{5}$$

Furthermore, the following attenuation factor is applied [24]:

$$\beta = \frac{2\pi f}{c}\sqrt{\frac{\kappa'\left(\sqrt{1+\tan^2\delta}-1\right)}{2}} \tag{6}$$

where f is the frequency of radiation, c is the light speed, κ' is the relative dielectric constant, and δ is the phase angle.

Having irradiation on the top and bottom surfaces, the corresponding boundary conditions for the microwave propagating along z-axis are given as follows:

$$E_{r,0}\big|_{z=0,L} = E_{r,1}\big|_{z=0,L} \tag{7}$$

$$\frac{1}{\mu_0\omega}\frac{dE_{r,0}}{dz}\bigg|_{z=0} = \frac{1}{\mu_1\omega}\frac{dE_{r,1}}{dz}\bigg|_{z=0} \tag{8}$$

where 0 and 1 indicate the free and medium (object) space, respectively, through which microwave propagates. Hence, the solution for Equation (4) can be written as follows:

$$E_{r,l} = A_l e^{i\chi_l z} + B_l e^{-i\chi_l z} E_{r,l} \tag{9}$$

where:

$$A_l = \frac{T_{01}E_0}{1+R_{01}e^{i\chi_l L}} \tag{10}$$

$$B_l = \frac{T_{01}E_0 e^{i\chi_l L}}{1+R_{01}e^{i\chi_l L}} \tag{11}$$

The transmission and reflection coefficients within the object are respectively given by

$$T_{01} = \frac{2\xi_1}{\xi_1+\xi_0} \tag{12}$$

$$R_{01} = \frac{\xi_1-\xi_0}{\xi_1+\xi_0} \tag{13}$$

where $\xi = \frac{\mu\omega}{\chi}$ is the intrinsic impedance, and $\omega = 2\pi f$ is the angular velocity. Then, the electric field distribution in the cylinder object is given by

$$E = \frac{T_{01}E_0}{1+R_{01}e^{i\chi_l L}}\left(e^{i\chi_l z} + e^{i\chi_l (L-z)}\right) \tag{14}$$

Following the same analysis, the corresponding boundary conditions for a slab are given by

$$E_0 = E_1 \tag{15}$$

$$\frac{1}{\mu_0\omega}\frac{dE_0}{dz} = \frac{1}{\mu_1\omega}\frac{dE_1}{dz} \tag{16}$$

One can then obtain the electric field distribution in a slab medium as

$$E = \frac{T_{01}E_0}{1 + R_{01}e^{i\chi_l b}}(e^{i\chi_l z} + e^{i\chi_l (b-z)}) \tag{17}$$

In Equations (22) and (25), L and b respectively represent the length of cylinder and thickness of slab.

2.2. Heat Transfer Due to Microwave Heating

Upon getting the expressions for electric field distribution, heat transfer analysis due to microwave heating can be carried out accordingly by taking into account heat generation (the power dissipated per unit volume) produced by the microwave heating [25] using the Poynting theorem as follows [21]:

$$\vec{q} = \frac{1}{2}\vec{E} \times \vec{H}^* \tag{18}$$

$$Q(z) = -\mathrm{Re}(\vec{\nabla} \cdot \vec{q}) \tag{19}$$

$$Q(z) = \frac{1}{2}\omega\varepsilon_0\kappa'' |E|^2 \tag{20}$$

By substituting Equation (9) into Equation (20), the power volumetric generation within a cylinder medium is obtained as

$$Q(z) = \frac{1}{2}\,\omega\varepsilon_0\kappa'' |E_0|^2 |T_{01}|^2 \times \frac{e^{-2\beta z} + e^{-2\beta(L-z)} + 2e^{-\beta L}\cos(2\sigma z - \sigma L)}{1 + 2|R_{01}|e^{-\beta L}\cos(\delta_{01} + \sigma L) + |R_{01}|^2 e^{-2\beta L}} \tag{21}$$

Furthermore, the power volumetric generation within a slab medium is obtained as

$$Q(z) = \frac{1}{2}\omega\varepsilon_0\kappa'' |E_0|^2 |T_{01}|^2 \times \frac{e^{-2\beta z} + e^{-2\beta(b-z)} + 2e^{-\beta L}\cos(2\sigma z - \sigma b)}{1 + 2|R_{01}|e^{-\beta b}\cos(\delta_{01} + \sigma L) + |R_{01}|^2 e^{-2\beta b}} \tag{22}$$

where κ'' is the relative dielectric loss.

The governing equation for heat transfer with a heat source can then be written as follows [26,27]:

$$\rho c_p \frac{dT}{dt} = \vec{\nabla} \cdot (k\vec{\nabla}T) + Q \tag{23}$$

where the heat sources for the cylinder and slab are taken from Equations (21) and (22), respectively. For a cylinder with outside radius r_0, the heat transfer equation due to the microwave heating can be written as follows:

$$\frac{\partial^2\theta}{\partial r^2} + \frac{1}{r}\frac{\partial\theta}{\partial r} + \frac{\partial^2\theta}{\partial z^2} + \frac{Q(z)}{k} = \frac{1}{\alpha}\frac{\partial\theta}{\partial t} \text{ for } 0 \le r \le r_0; 0 < z < L \tag{24}$$

along with the following initial and boundary conditions:

$$T = T_i \text{ for } t = 0 \tag{25}$$

$$-k\frac{\partial T}{\partial r} = h(T - T_\infty) \text{ on } r = r_0 \tag{26}$$

$$k\frac{\partial T}{\partial z} = h(T - T_\infty) \text{ on } z = 0 \tag{27}$$

$$-k\frac{\partial T}{\partial z} = h(T - T_\infty) \text{ on } z = L \tag{28}$$

The above equations and boundary conditions are solved using the FE method in the present research study.

2.3. Procedures for Microwave Heating Using FEM

Numerical steps performed in this work include the following:

(i) Verification was carried out for FE simulation, with microwave heating problems having well-known analytical solutions in order to ensure the robustness of the FE simulation. Microwave heating results on cylindrical beef and a salmon slab were used here as verification problems [22,23].

(ii) Afterward, FE simulations for microwave heating on ilmenite samples having cylinder and slab shapes were carried out, with variation of sample height. It is noted here that related material properties (in SI (International System of Units) units) for samples undergoing microwave heating were taken from available literature.

(iii) The obtained simulation results were corroborated with available data in the literature for ilmenite processing using microwave heating.

For step (i), analytical solutions for the microwave heating problems are available. For compactness of presentation, the detailed derivation for such analytical solutions is omitted here. Readers may refer to References [22,23] for further details. A modified temperature variable is introduced inside the cylinder and slab by

$$\theta(r,z,t) = T(r,z,t) - T_\infty \tag{29}$$

$$\theta(x,y,z,t) = T(x,y,z,t) - T_\infty \tag{30}$$

Then, the analytical solutions for temperature distribution inside the cylinder and slab shapes due to microwave heating are given as follows:

$$\theta(r,z,t) = \sum_{m=1}^{\infty}\sum_{n=1}^{\infty} \frac{{\lambda_m}^2 J_0(\lambda_m r)(\eta_n \cos\ \eta_n z + \gamma \sin\ \eta_n z)}{[{r_0}^2 {J_0}^2(\lambda_m r_0)(\gamma^2+{\lambda_m}^2)][L({\eta_n}^2+\gamma^2)+2\gamma]} \overset{=}{\theta}(\lambda_m,\eta_n,t) \tag{31}$$

$$\begin{aligned}\theta(x,y,z,t) = {} & \sum_{n=1}^{\infty}\sum_{p=1}^{\infty}\sum_{q=1}^{\infty} A\left(\lambda_n,\xi_p,\eta_q,x,y,z\right) \\ & \times \left[\frac{\Phi(x,y,z,t-\tau)}{\alpha\left({\lambda_n}^2+{\xi_p}^2+{\eta_q}^2\right)}\left(1-e^{-\alpha({\lambda_n}^2+{\xi_p}^2+{\eta_q}^2)\tau}\right)\right] \\ & + \sum_{n=1}^{\infty}\sum_{p=1}^{\infty}\sum_{q=1}^{\infty} A\left(\lambda_n,\xi_p,\eta_q,x,y,z\right) \\ & \times C\left(\lambda_n,\xi_p,\eta_q,a,w,b,\theta(x,y,z,t-\tau)\right)e^{-\alpha({\lambda_n}^2+{\xi_p}^2+{\eta_q}^2)\tau}\end{aligned} \tag{32}$$

for any position inside (r and z for cylinder and x, y, and z for slab) and related time t, where J_0 is the characteristic function, λ_m represents the eigen-values from the characteristic function, γ is the ratio between coefficient h and thermal conductivity k, η_n represents the eigen-values in the z-direction from Fourier transform, α is the thermal diffusity, and τ is the period of electromagnetic heating. For variables Φ, A, and C, readers are further directed to References [22,23].

It is also noted here that the value of τ needs to be determined by the user. In addition, it may be expected that, for a given cross-sectional area, the sample height/thickness would be related to the effectiveness of microwave heating and uniformity of temperature distribution in relation to penetration depth of microwave radiation.

Accordingly, FE equations for the thermal problem including heat source are given as follows [28]:

$$[\mathrm{C}]\left\{\dot{T}\right\} + [\mathrm{K}]\{T\} = \{F_T\} \tag{33}$$

$$[\mathrm{C}] = \int_V \rho c_p [\mathrm{N}]^T \{\mathrm{N}\} dV \tag{34}$$

$$[\mathrm{K}] = \int_V k[\mathrm{B}]^T\{\mathrm{B}\}dV + \int_S h[\mathrm{N}]^T\{\mathrm{N}\}dS \quad (35)$$

$$\{F_T\} = \int_V Q[\mathrm{N}]^T dV + \int_S hT_{ref}[\mathrm{N}]^T dS \quad (36)$$

where [N] is the matrix of the shape function, [B] is the matrix of the shape function derivative, and $\{T\}$ is the vector of nodal temperatures, while h is the convection coefficient and T_{ref} is the reference temperature.

Here, Tables 1–3 describe material properties employed in the present research work.

Table 1. Thermal and dielectric properties of cylindrical beef (f = 2450 MHz) [21,22].

Properties	Values
Thermal conductivity, k (W/mK)	0.466
Specific heat capacity, c_p (J/kgK)	3200
Density, ρ (kg/m^3)	1030
Dielectric constant, κ'	30.5
Dielectric loss, κ''	9.6
Transmission coefficient, $\|T_{01}\|$	0.301
Reflection coefficient, $\|R_{01}\|$	0.7026
Phase angle, δ_{01} (rad)	−3.09
Phase factor, σ (rad/m)	288
Attenuation factor, β (rad/m)	44.2

Table 2. Thermal and dielectric properties of salmon fillets (f = 2450 MHz).

Properties	Values
Thermal conductivity, k (W/mK) [23]	0.4711
Specific heat capacity, c_p (J/kgK) [23]	3589.4
Density, ρ (kg/m^3) [23]	1047.89
Transmission coefficient, $\|T_{01}\|$ [29]	0.243
Reflection coefficient, $\|R_{01}\|$ [29]	0.761
Phase angle, δ_{01} (rad) [29]	3.095
Phase factor, σ (rad/m) [29]	367.32
Attenuation factor, β(rad/m) [29]	61.65
Dielectric constant, κ' [23]	51.2
Dielectric loss, κ'' [23]	18.24

Table 3. Dielectric and material properties of ilmenite (f = 2450 MHz) [30,31].

Properties	Values
Dielectric constant, κ'	16.8
Dielectric loss, κ''	8.6
Phase angle, δ_{01} (rad)	2.93
Phase factor, σ (rad/m)	210.4
Attenuation factor, β (rad/m)	61.286
Transmission coefficient, $\|T_{01}\|$	0.4602
Reflection coefficient, $\|R_{01}\|$	0.0045

Furthermore, temperature-dependent material properties of thermal conductivity and specific heat for ilmenite were used in the FE simulation, taken from References [32,33]. All FE simulations were realized using ANSYS v17 software (ANSYS, Canonsburg, PA, USA).

3. Results

3.1. Verification of FE Simulation

In this section, numerical parameters used were the incidence microwave energy flux $I = 3$ W/cm^2 (corresponding to a 1.2-kW household microwave), $h = 10$ W/m^{2}K, radius of cylindrical beef $r_0 = 0.005$ m, and height/thickness of cylindrical beef $L = 0.0125$ m. Initial uniform temperature T_0 was taken as 298 K. Final time t was taken at 120 s for comparison purposes. Due to symmetry, only a half-model was used. The number of elements employed was 245,760 elements. For the FE simulation with the slab, the parameters were the incidence microwave energy flux $I = 3$ W/cm^2 (corresponding to a 1.2-kW household microwave), $h = 10$ W/m^{2}K, dimension of salmon fillet of length × width × thickness = 0.07 m × 0.04 m × 0.015 m. Initial uniform temperature T_0 was taken as 298 K. Final time t was taken at 75 s. Similarly, due to symmetry, only a half-model was used. The number of elements employed was 168,000 elements. It is noted here that the simulation results previously presented in Reference [34] for a cylinder of beef were extended by adding the FE results for a slab of salmon, thus showing the applicability of numerical simulations using FEM for investigating a wide range of microwave heating problems and applications.

Results of verification for the FE simulation are shown in Figure 2a–c. Figure 2a depicts the FE simulation results of temperature profiles along the axial center of cylindrical beef with respect to the variation of microwave heating times. Figure 2b shows the FE simulation results of temperature profiles along the axial center of salmon slab with respect to the variation of microwave heating times. In addition, Figure 2c shows relative errors between temperature values along the axial center of salmon slab obtained from FE simulation and the analytical solution.

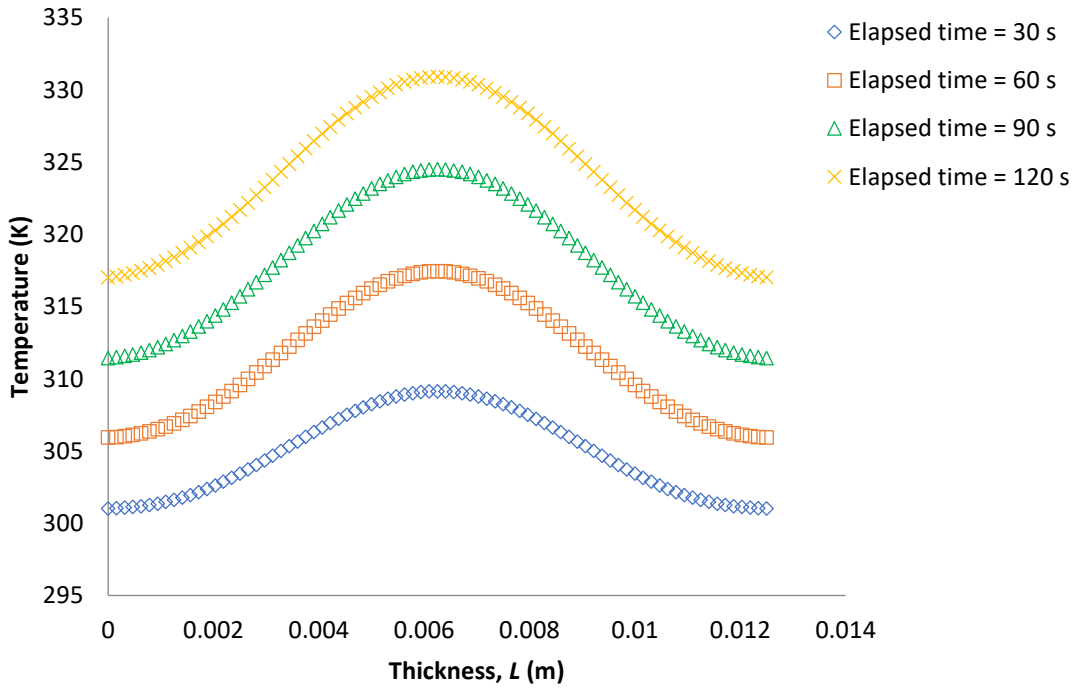

(**a**)

Figure 2. *Cont.*

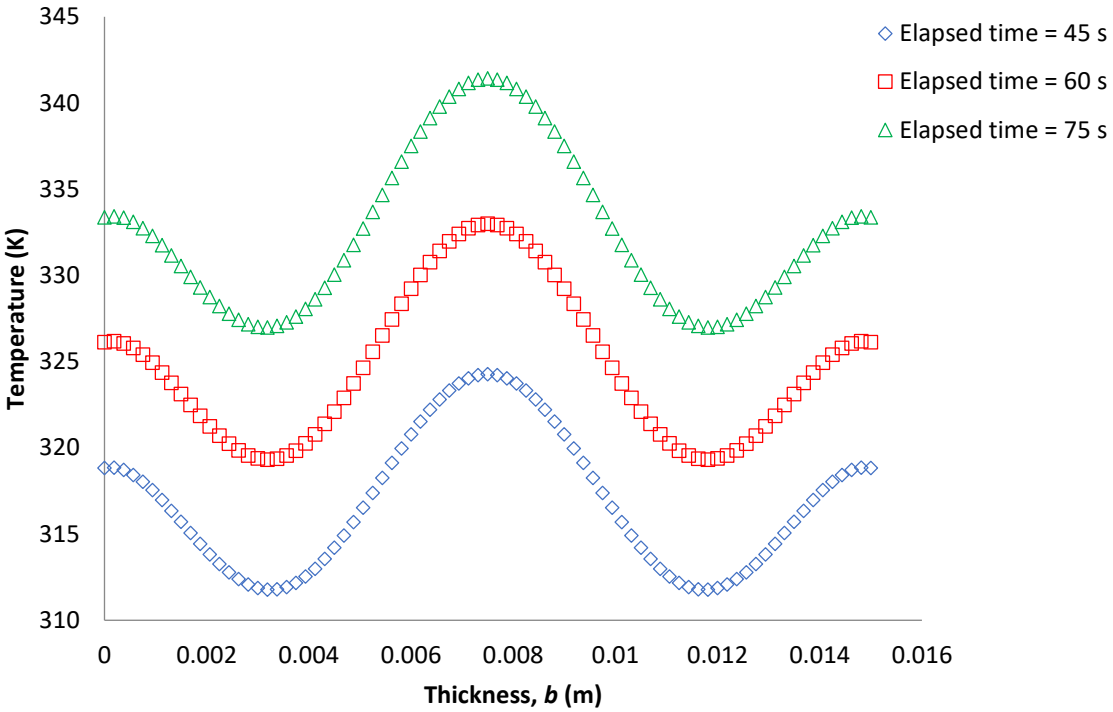

(**b**)

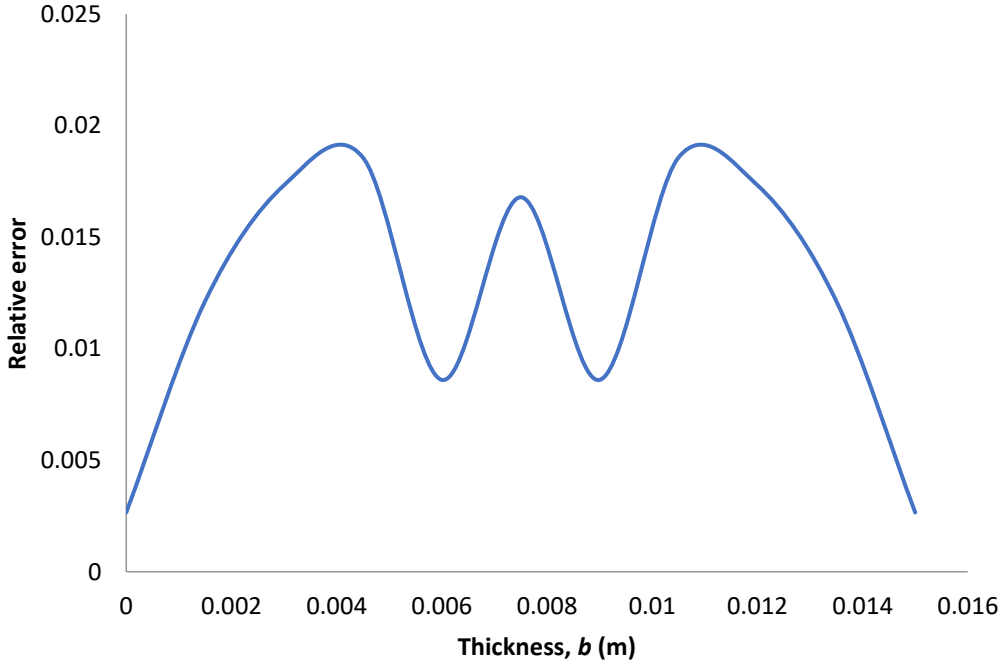

(**c**)

Figure 2. Verification of finite element (FE) simulation: (**a**) results of temperature profiles along the axial center of cylindrical beef with respect to the variation of microwave heating times; (**b**) results of temperature profiles along the axial center of salmon slab with respect to the variation of microwave heating times; (**c**) relative errors between temperatures along the axial center of salmon slab obtained from FE simulation and the analytical solution.

From Figure 2a–c, one can note the good agreement between FE solutions for this microwave heating problem and the corresponding exact solutions. The average relative error between FE simulation and analytical solution for the temperature profile of cylinder geometry was 0.13%, while it was 1.2% for the slab geometry. Hence, it can be said that the FE simulation performed in this study was verified with good numerical performance and accuracy. In subsequent sections, the numerical procedures are used to evaluate temperature distributions inside the ilmenite samples due to microwave heating treatment.

3.2. Simulation Results for Ilmenite Sample with Cylinder Shape

In this section, numerical results of temperature distribution in the ilmenite sample of cylinder shape due to microwave heating are presented. Parameters used were the incidence microwave energy flux I = 13.875 W/cm^2 (corresponding to a 5.55-kW microwave batch furnace), h = 10 W/m^{2}K, and radius of cylindrical ilmenite r_0 = 0.035 m, with the variation of height/thickness L = 0.015, 0.03, 0.045, and 0.06 m. Initial uniform temperature T_0 was taken as 298 K. Final time t was taken as 240 s (4 min), with a time interval of 60 s.

Figure 3 presents the temperature distribution inside the cylindrical ilmenite after being heated for 4 min with respect to the variation of cylinder height. Moreover, profiles of heat generation along the center line of cylindrical ilmenite due to microwave heating with respect to the variation of cylinder heights are depicted in Figure 4. In Figure A1 (Appendix A), temperature profiles along the center line of cylindrical ilmenite with respect to the variation of microwave heating times for different thickness are shown. Note that the simulation results for the cylindrical ilmenite were also reported previously in Reference [34], but they are represented here for clarity of comparison with the FE simulation results obtained for the slab of ilmenite.

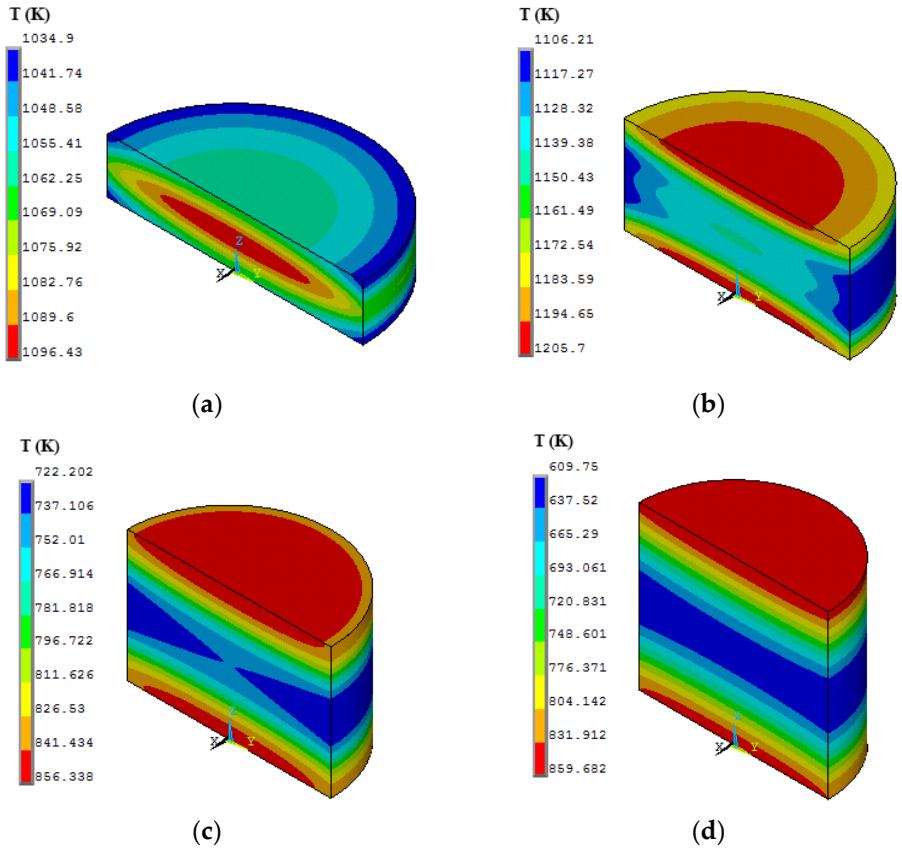

Figure 3. Temperature distribution inside the cylindrical ilmenite after being heated for 4 min with the variation of cylinder height: (**a**) L =0.015 m; (**b**) L = 0.03 m; (**c**) L = 0.045 m; (**d**) L = 0.06 m.

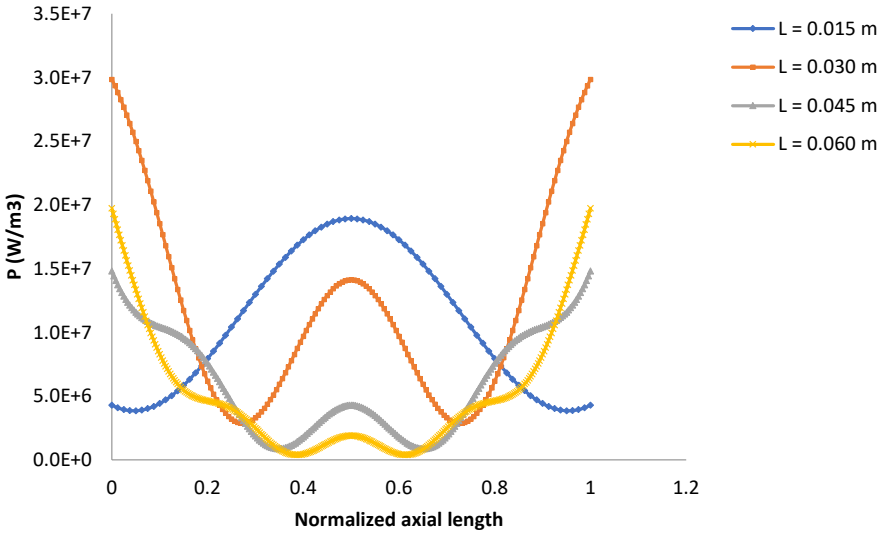

Figure 4. Profiles of heat generation along the center line of cylindrical ilmenite due to microwave heating with respect to the variation of cylinder thickness.

3.3. Simulation Results for Ilmenite Sample with Slab Shape

Figure 5 presents temperature distribution inside the ilmenite slab after being heated for 4 min with respect to the variation of slab height. In Figure A2 (Appendix A), temperature profiles along the center line of ilmenite slab with respect to the variation of microwave heating times are shown for different thickness values.

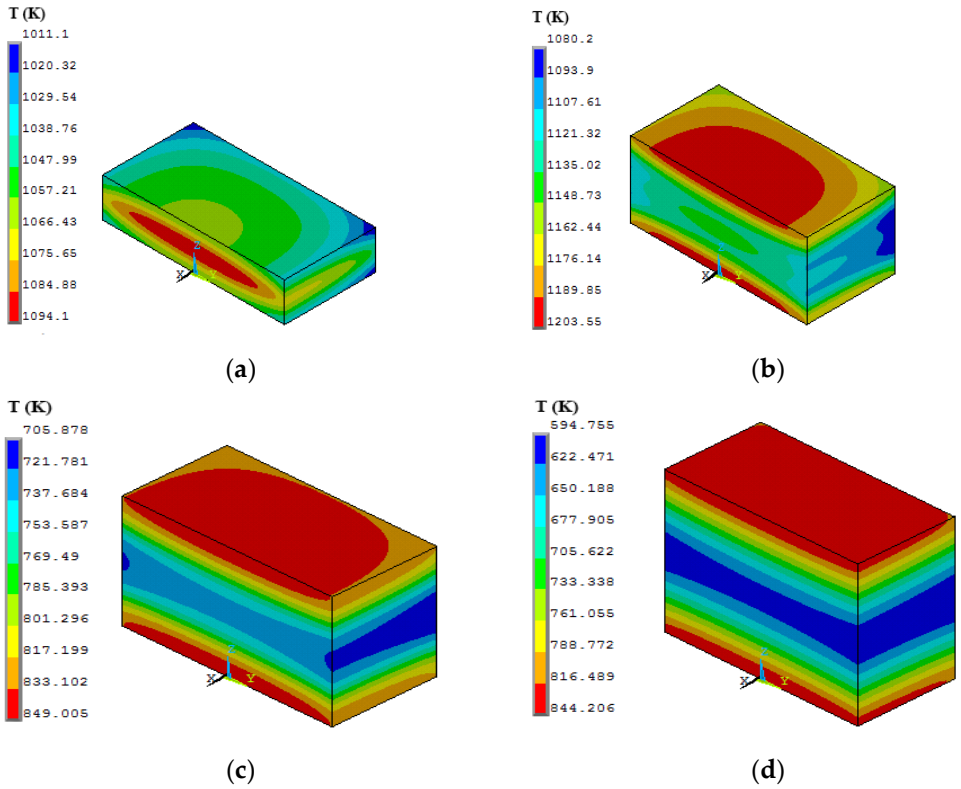

Figure 5. Temperature distribution inside the ilmenite slab after being heated for 4 min with the variation of slab height: (**a**) b =0.015 m; (**b**) b = 0.03 m; (**c**) b = 0.045 m; (**d**) b = 0.06 m.

For the slab of ilmenite, parameters used in the simulation were the incidence microwave energy flux I = 13.875 W/cm^2 (corresponding to a 5.55-kW microwave batch furnace), h = 10 W/m^{2}K, and

dimension of slab base area of length × width = 0.07 m × 0.07 m, with the variation of height/thickness b = 0.015, 0.03, 0.045, and 0.06 m. Initial uniform temperature T_0 was taken as 298 K. Final time t was taken as 240 s (4 min), with a time interval of 60 s.

4. Discussion

Based on the FE simulations of microwave heating on ilmenite samples with comparable characteristic length, the results presented above are discussed here. The discussion is elaborated with respect to maximum temperature attained, temperature differences, and uniformity of temperature inside the ilmenite samples.

From Figure 3, temperature differences between maximum and minimum temperatures for the cylindrical ilmenite were 61.53 K, 99.49 K, 134.14 K, and 249.93 K for thickness values L of 0.015 m, 0.03 m, 0.045 m, and 0.06 m, respectively. For the ilmenite slabs, the temperature differences were respectively 83 K, 123.35 K, 143.13 K, and 249.45 K, as shown in Figure 5. It can be observed that temperature differences in the slabs were generally greater than those in the cylindrical samples with the thickness variation. A minor exception was, however, observed for the thickness value of 6 cm, i.e., the largest thickness, in which the temperature difference was almost the same. While the profiles of temperature inside the ilmenite samples were similar for both geometries as depicted in Figures A1 and A2 (Appendix A), it can be said that the slab geometry induced greater non-uniformity of temperature inside the ilmenite, for the same duration of microwave heating.

It was also observed that, for the ilmenite samples with thickness value greater than 1.5 cm, the hotspot locations were not in the center of sample, but on the surface of sample.

The results above may suggest that a certain thickness value is preferred for ilmenite heating. Thicker samples may not be preferred as the temperature differences produced are large, thus inducing greater non-uniformity of temperature in the samples. Moreover, thicker samples may need longer heating time to attain proper temperature values for the ilmenite to be decomposed into Fe and TiO_2 (around 950–1000 °C). On the other hand, thinner samples can attain the maximum temperature value, but one should consider that local melting in the sample (i.e., in the ore matrix) may occur due to hotspots at the considerably high temperature of 1100 °C [12,14]. The simulation results indeed show that ilmenite sample with a thickness value of 3 cm gave a good trade-off between the maximum temperature attained and temperature differences inside the ilmenite sample, for both geometries. The results can also be verified from Figure 4. It shows that the power dissipated per unit volume for the ilmenite sample with a thickness of 3 cm was the largest.

Furthermore, while thinner samples can attain higher temperature values, it can be observed that thicker samples can attain a more uniform temperature on their respective layered/sliced planes, especially at the end of the heating duration of 4 min. This can be seen in Figures 3 and 5.

It is also interesting to note that the hotspot location in the ilmenite changed as the thickness of sample was varied. Figure 4 depicts this observation. The maximum temperature for the thinnest sample took place at the center of sample. Conversely, the maximum temperature occurred at the top and bottom surfaces of the sample for thicker samples. This means that the hotspots moved to the surface as the thickness increased. This observation is consistent with the FE simulation results presented in Reference [35]. The consequences are that one cannot expect the uniformity of temperature inside the ilmenite samples, unless giving some rotation to the samples [35].

Finally, Table 4 summarizes maximum and minimum temperatures attained in the ilmenite samples of cylinder and slab shapes after heating for 4 min using the 5.55-kW microwave batch furnace. Although the experimental conditions and parameters were not identical with those of the present simulation, the relationship obtained from the experiment in Reference [14] was employed here to assess the consistency of this study. In Reference [14], a sample of 500 g of ilmenite ore (low grade) was dried at 105 °C for 2 h and then was placed in a crucible (made of ceramic with dimensions of inner diameter of 100 mm and a length of 200 mm). A thermocouple pyrometer was inserted into the center of the sample for taking temperature measurements. Microwave radiation was imposed on the

sample. The power intensity of microwave heating used was in the range of 0–3 kW with a frequency of 2450 MHz. After a preset residence time, the microwave irradiation was stopped, and temperature was recorded. The experiment produced the following relationship between the temperature of the ilmenite sample and microwave heating times: $T = 111.7214 + 62.32872t - 1.4069t^2 + 0.01247t^3$, where T is the ilmenite sample temperature (at the center, in °C) and t is heating time (in minutes). The temperature value obtained from the relationship is shown in Table 4, by taking $t = 4$ min.

Table 4. Maximum and minimum temperatures attained in the ilmenite samples with cylinder and slab shapes after heating for 4 min using the 5.55-kW microwave batch furnace.

Ilmenite Samples	Sample Thickness (cm)	Maximum Temperature (°C)	Minimum Temperature (°C)	Difference of Temperatures (°C)	Temperature from the Relationship in Reference [14] (°C)
Cylinder	1.5	823.28	761.75	61.53	612.32
	3.0	932.55	833.06	99.49	
	4.5	583.19	449.05	134.14	
	6.0	586.53	336.60	249.93	
Slab	1.5	820.95	737.95	83	
	3.0	930.40	807.05	123.35	
	4.5	575.86	432.73	143.13	
	6.0	571.06	321.61	249.45	

Despite the lack of information concerning the precise value of sample thickness in Reference [14], it can be observed that the maximum and minimum temperatures attained in the samples from the FE simulations were around the temperature value obtained from the relationship in Reference [14]. In addition, the experiment also showed that the optimum dimensions for microwave heat deposition were uniform in a sample being irradiated from both sides in a 2450-MHz microwave when varied from 5 to 10 cm. The dimensions considered in the present study are, therefore, consistent with the reported dimensions.

5. Conclusions

In this study, numerical simulations of microwave heating for ilmenite processing were presented using the FE method. Numerical results showed that the shape and thickness of ilmenite samples affected the effectiveness of microwave heating of ilmenite, in terms of maximum temperature attained, temperature differences, and uniformity of temperature. Temperature distributions inside the ilmenite samples under the microwave heating process were clearly visualized in this study, upon following proper verification steps for the simulation. The visualization highlighted penetration depth of the microwave during heating, as well as different hotspot locations for samples with different thickness values, which appear to be consistent with other studies in the literature. The effects of power intensity value, heating times, and optimization among several variables in the microwave heating process for mineral processing may be interesting subjects of investigation in future study.

Author Contributions: Methodology and writing—original draft, M.I.P.H.; software, F.I.R.; resources, D.M.F. and A.M. All authors have read and agreed to the published version of the manuscript.

Funding: This work was supported by the PTUPT grant (5/E1/KP.PTNBH/2019) from the Ministry of Research, Technology, and Higher Education of the Republic of Indonesia (Kemenristek DIKTI).

Acknowledgments: Support from ITS Surabaya is gratefully acknowledged.

Conflicts of Interest: The authors declare no conflicts of interest.

Appendix A

For clarity of manuscript presentation, some figures are placed in this appendix section.

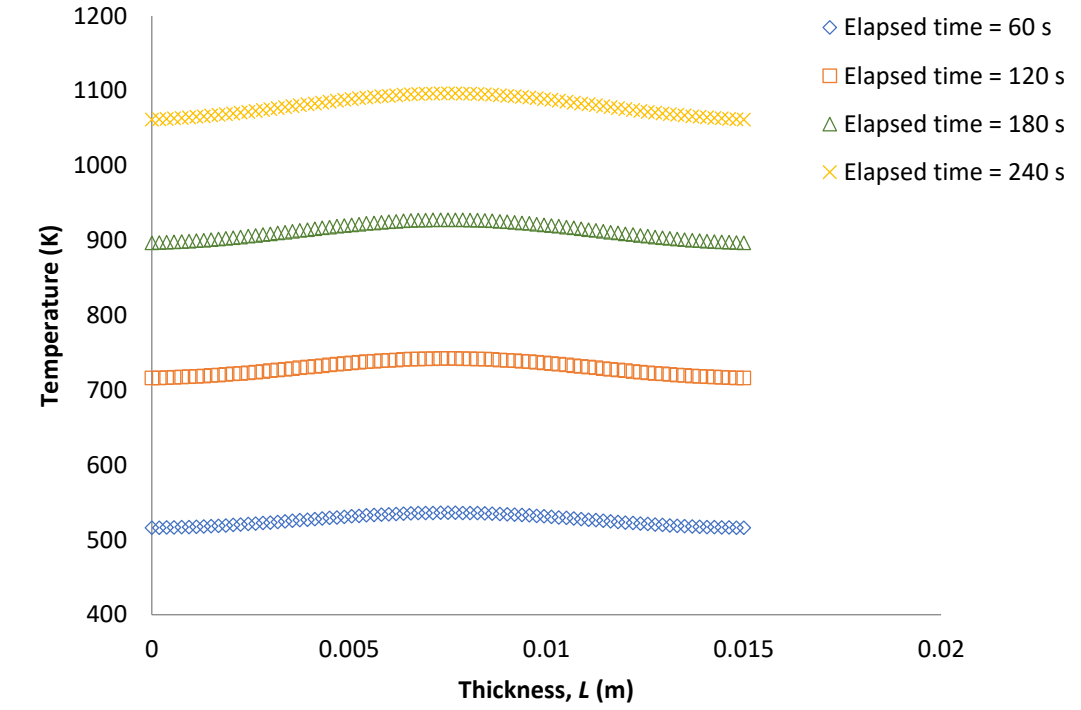

(**a**)

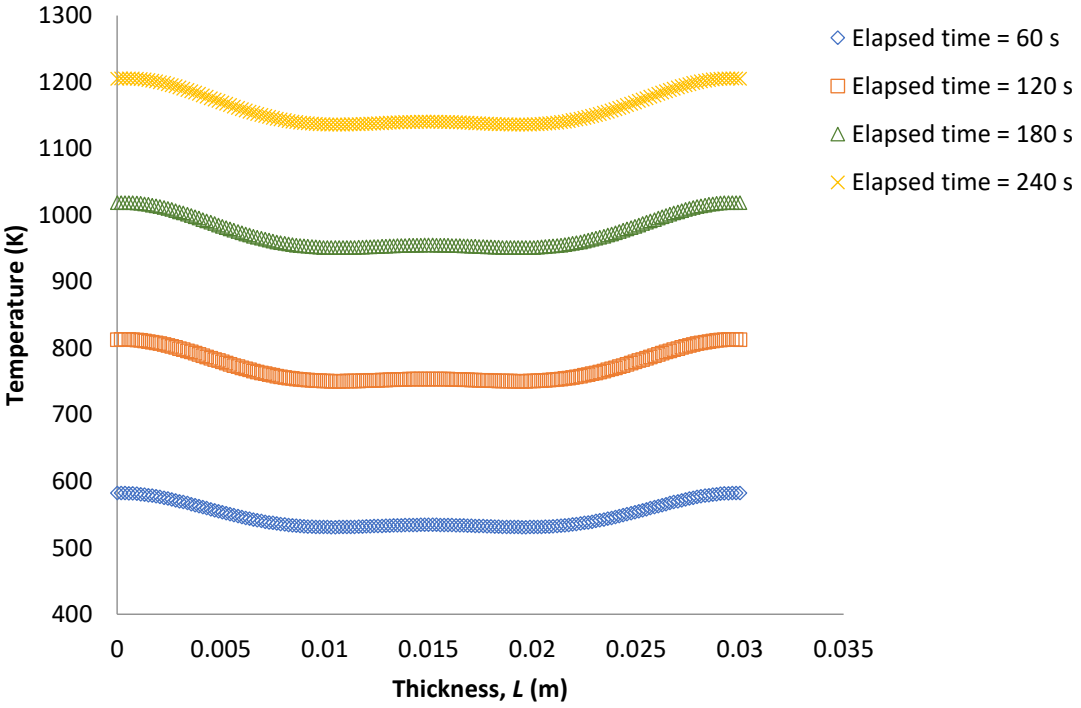

(**b**)

Figure A1. *Cont.*

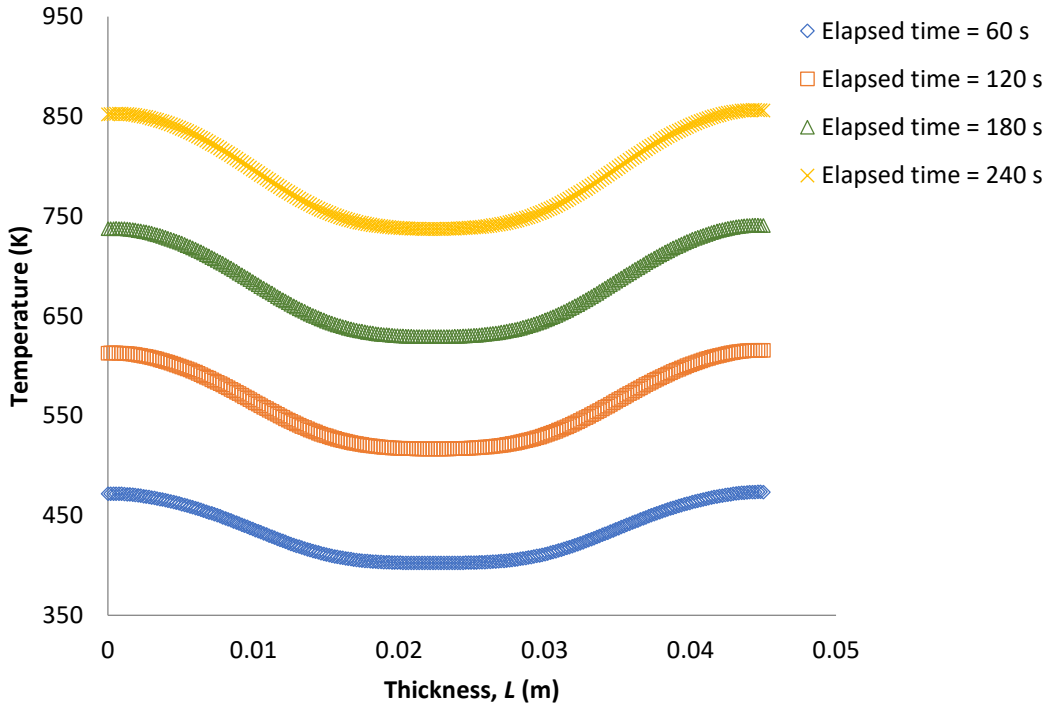

(**c**)

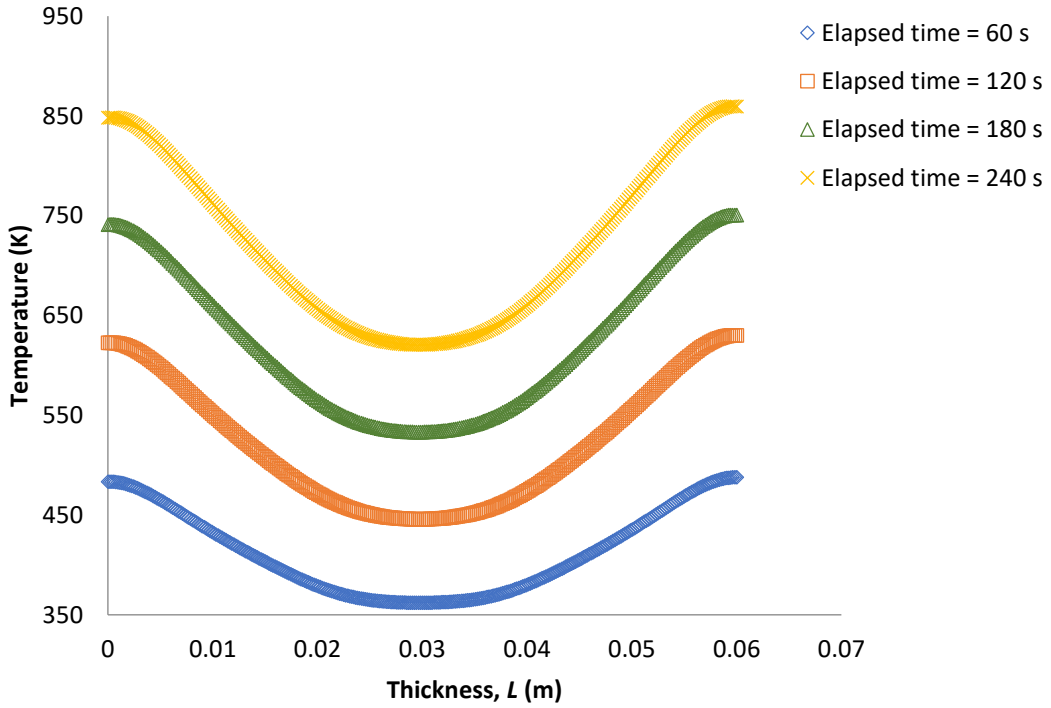

(**d**)

Figure A1. Temperature profiles along the center line of cylindrical ilmenite with respect to the variation of microwave heating times for different thickness: (**a**) L = 0.015 m; (**b**) L = 0.03 m; (**c**) L = 0.045 m; (**d**) L = 0.06 m.

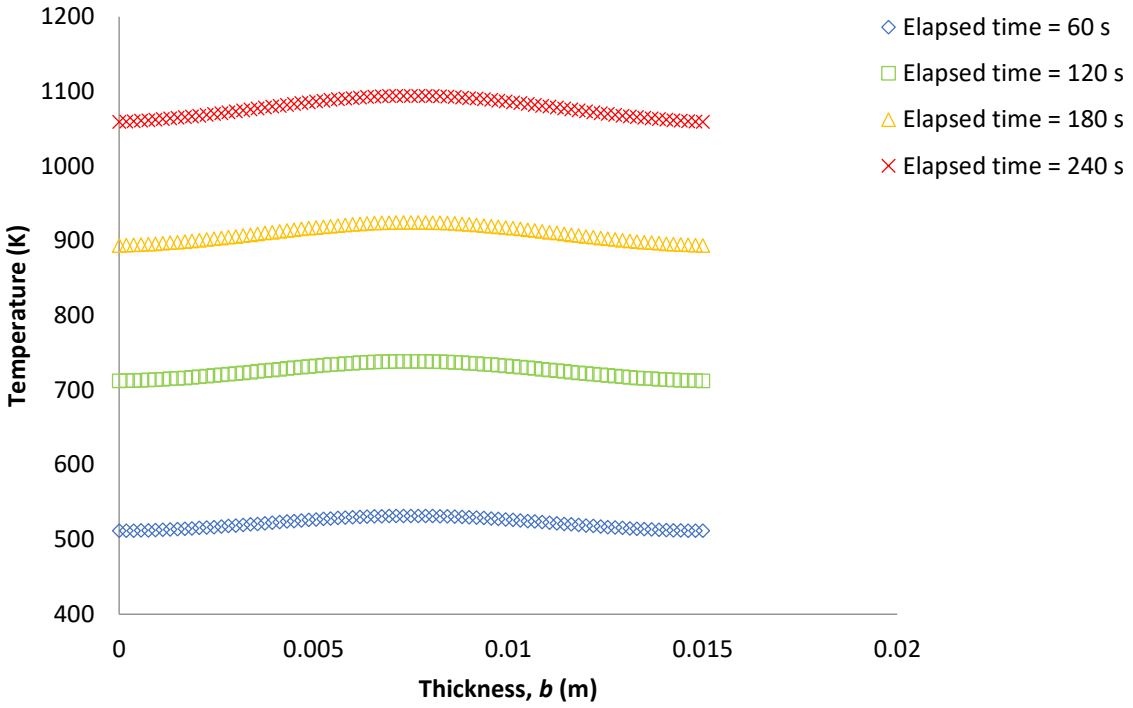

(**a**)

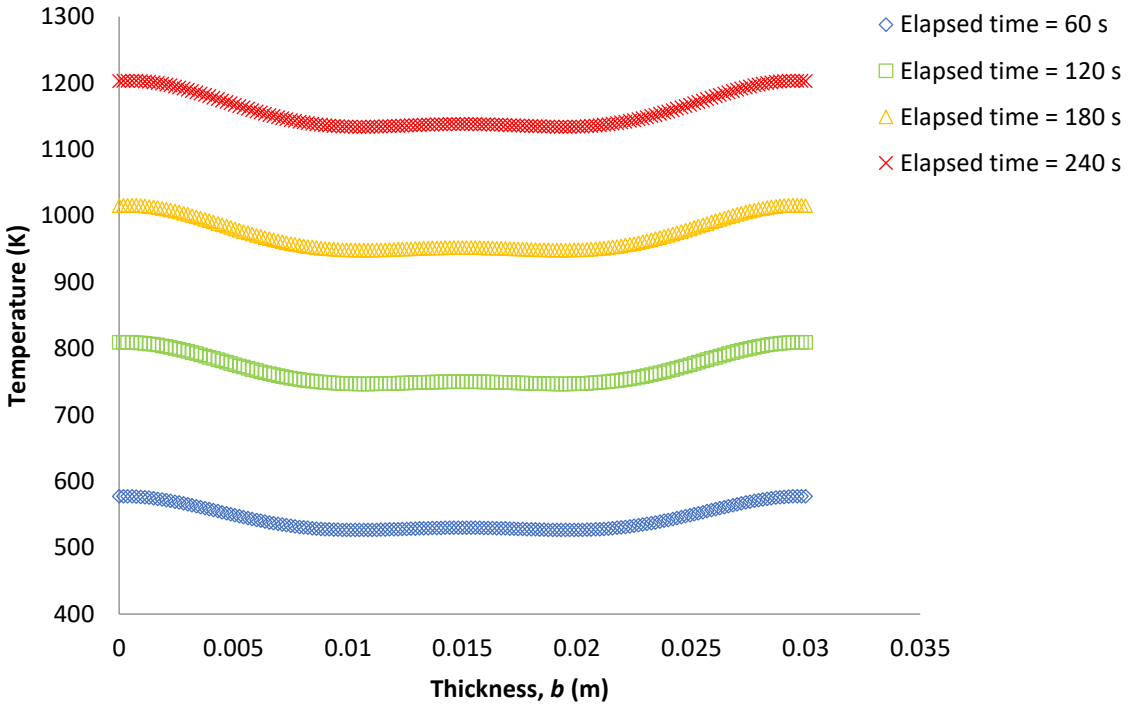

(**b**)

Figure A2. *Cont.*

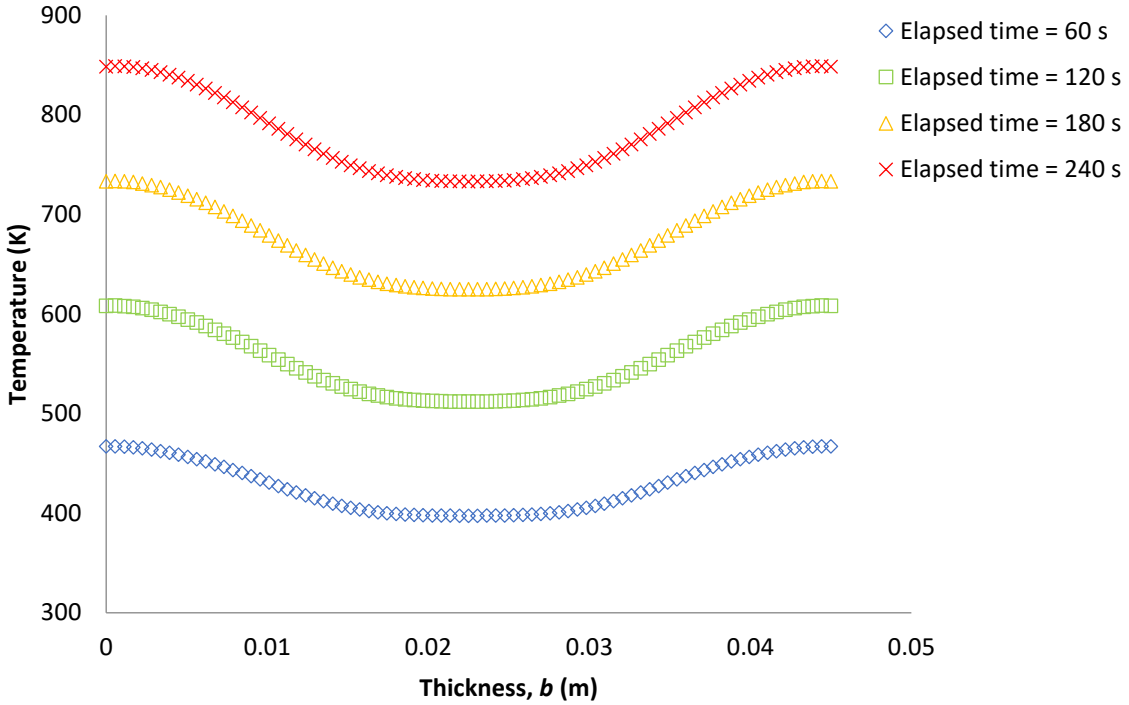

(**c**)

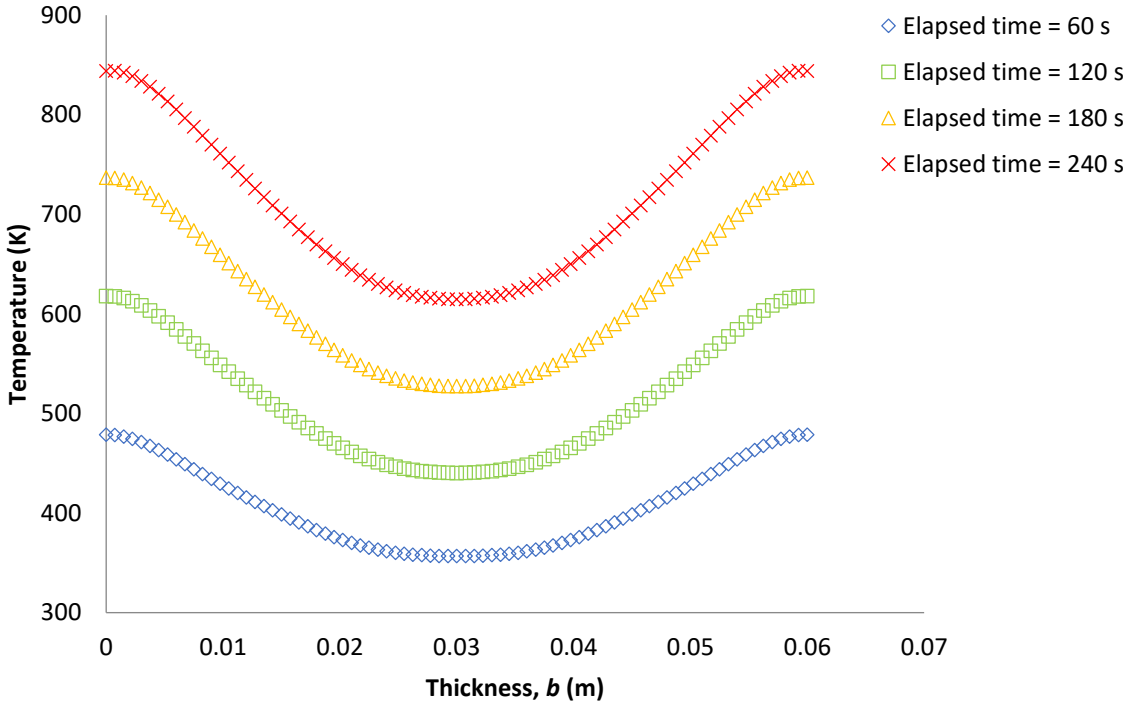

(**d**)

Figure A2. Temperature profiles along the center line of ilmenite slab with respect to the variation of microwave heating times for different thickness: (**a**) b = 0.015 m; (**b**) b = 0.03 m; (**c**) b = 0.045 m; (**d**) b = 0.06 m.

References

1. Thostenson, E.; Chou, T.-W. Microwave processing: Fundamentals and applications. *Compos. Part A* **1999**, *30*, 1055–1071. [CrossRef]
2. Zhu, Y.-J.; Chen, F. Microwave-Assisted Preparation of Inorganic Nanostructures in Liquid Phase. *Chem. Rev.* **2014**, *114*, 6462–6555. [CrossRef]
3. Mishra, R.R.; Sharma, A.K. Microwave–material interaction phenomena: Heating mechanisms, challenges and opportunities in material processing. *Compos. Part A* **2016**, *81*, 78–97. [CrossRef]
4. Sun, J.; Wang, W.; Yue, Q. Review on Microwave-Matter Interaction Fundamentals and Efficient Microwave-Associated Heating Strategies. *Materials* **2016**, *9*, 231. [CrossRef]
5. Vadivambal, R.; Jayas, D.S. Non-uniform Temperature Distribution During Microwave Heating of Food Materials—A Review. *Food Bioprocess Technol.* **2008**, *3*, 161–171. [CrossRef]
6. Liao, Y.; Lan, J.; Zhang, C.; Hong, T.; Yang, Y.; Huang, K.M.; Zhu, H. A Phase-Shifting Method for Improving the Heating Uniformity of Microwave Processing Materials. *Materials* **2016**, *9*, 309. [CrossRef]
7. Pusat Sumber Daya Mineral Batubara dan Panas Bumi-Badan Geologi. Kementerian Energi dan Sumber Daya Mineral. 2019. Available online: http://psdg.geologi.esdm.go.id/index.php (accessed on 1 March 2020).
8. Barksdale, J. Titanium, Its Occurrence, Chemistry, and Technology. *Soil Sci.* **1950**, *70*, 414. [CrossRef]
9. Kelly, R.; Rowson, N. Microwave reduction of oxidised ilmenite concentrates. *Miner. Eng.* **1995**, *8*, 1427–1438. [CrossRef]
10. Gupta, S.K.; Rajakumar, V.; Grieveson, P. Phase transformations during heating of llmenite concentrates. *Met. Mater. Trans. A* **1991**, *22*, 711–716. [CrossRef]
11. Francis, A.; El-Midany, A.; El-Midany, A. An assessment of the carbothermic reduction of ilmenite ore by statistical design. *J. Mater. Process. Technol.* **2008**, *199*, 279–286. [CrossRef]
12. Kingman, S.; Corfield, G.M.; Rowson, N. Effects of Microwave Radiation Upon the Mineralogy and Magnetic Processing of a Massive Norwegian Ilmenite Ore. *Magn. Electr. Sep.* **1999**, *9*, 131–148. [CrossRef]
13. Guo, S.; Chen, G.; Peng, J.; Chen, J.; Li, D.-B.; Liu, L.-J. Microwave assisted grinding of ilmenite ore. *Trans. Nonferrous Met. Soc. China* **2011**, *21*, 2122–2126. [CrossRef]
14. Liu, C.; Zhang, L.-B.; Peng, J.; Liu, B.; Xia, H.-Y.; Gu, X.-C.; Shi, Y.-F. Effect of temperature on dielectric property and microwave heating behavior of low grade Panzhihua ilmenite ore. *Trans. Nonferrous Met. Soc. China* **2013**, *23*, 3462–3469. [CrossRef]
15. Wang, X.; Li, W.; Yang, B.; Guo, S.; Zhang, L.-B.; Chen, G.; Peng, J.; Luo, H. Microwave-Absorbing of Carbothermic Reduced Products of Ilmenite and Oxidized Ilmenite. *J. Microw. Power Electromagn. Energy* **2014**, *48*, 192–202. [CrossRef]
16. Zhou, L.; Puri, V.; Anantheswaran, R.; Yeh, G. Finite element modeling of heat and mass transfer in food materials during microwave heating—Model development and validation. *J. Food Eng.* **1995**, *25*, 509–529. [CrossRef]
17. Lin, Y.; Anantheswaran, R.; Puri, V. Finite element analysis of microwave heating of solid foods. *J. Food Eng.* **1995**, *25*, 85–112. [CrossRef]
18. Dev, S.; Gariepy, Y.; Orsat, V.; Raghavan, G. Finite element modeling for optimization of microwave heating of in-shell eggs and experimental validation. *Int. J. Numer. Model. Electron. Netw. Devices Fields* **2011**, *25*, 275–287. [CrossRef]
19. Reinosa, J.J.; García-Baños, B.; Catalá-Civera, J.; Fernández, J.F. A step ahead on efficient microwave heating for kaolinite. *Appl. Clay Sci.* **2019**, *168*, 237–243. [CrossRef]
20. Shiah, Y.C.; Chaing, Y.-C.; Matsumoto, T. Analytical transformation of volume integral for the time-stepping BEM analysis of 2D transient heat conduction in anisotropic media. *Eng. Anal. Bound. Elem.* **2016**, *64*, 101–110. [CrossRef]
21. Roussy, G.; Pearce, J. *Foundations and Industrial Applications of Microwaves and Radio Frequency Fields. Physical and Chemical Processes*; Institute of Electrical and Electronics Engineers (IEEE): Piscataway, NJ, USA, 2005; Volume 1, pp. 115–116.
22. Hossan, M.; Byun, Y.; Dutta, P. Analysis of microwave heating for cylindrical shaped objects. *Int. J. Heat Mass Transf.* **2010**, *53*, 5129–5138. [CrossRef]
23. Hossan, M.; Dutta, P. Effects of temperature dependent properties in electromagnetic heating. *Int. J. Heat Mass Transf.* **2012**, *55*, 3412–3422. [CrossRef]

24. Ayappa, K.; Davis, H.; Crapiste, G.; Davis, E.; Gordon, J. Microwave heating: An evaluation of power formulations. *Chem. Eng. Sci.* **1991**, *46*, 1005–1016. [CrossRef]
25. Peng, Z. Heat Transfer in Microwave Heating. Ph.D. Theis, Michigan Technological University, Houghton, MI, USA, 2012. Available online: https://digitalcommons.mtu.edu/cgi/viewcontent.cgi?article=1016&context=etds&httpsredir=1&referer= (accessed on 21 April 2020).
26. Hidayat, M.I.P.; Ariwahjoedi, B.; Parman, S.; Rao, T. Meshless Local B-Spline Collocation Method for Two-Dimensional Heat Conduction Problems with Nonhomogenous and Time-Dependent Heat Sources. *J. Heat Transf.* **2017**, *139*, 071302. [CrossRef]
27. Hidayat, M.I.P. Meshless local B-spline collocation method for heterogeneous heat conduction problems. *Eng. Anal. Bound. Elem.* **2019**, *101*, 76–88. [CrossRef]
28. Bathe, K.J. *Finite Element Procedures*; Prentice-Hall, Inc.: Upper Saddle River, NJ, USA, 1996.
29. Wang, Y.; Tang, J.; Rasco, B.; Kong, F.; Wang, S. Dielectric properties of salmon fillets as a function of temperature and composition. *J. Food Eng.* **2008**, *87*, 236–246. [CrossRef]
30. Chiteme, C.; Mulaba-Bafubiandi, A.F. An investigation on electrical properties of microwave treated natural ilmenite (FeTiO3). *J. Mater. Sci.* **2006**, *41*, 2365–2372. [CrossRef]
31. Mindat.org, the Mineral and Locality Database Home Page. Available online: http://www.mindat.org/ (accessed on 31 May 2012).
32. Touloukian, Y.S. *Thermophysical Properties of Matter Volume 2: Thermal Conductivity Non Metallic Solid*; Plenum Publishing Corporation: New York, NY, USA, 1970.
33. Touloukian, Y.S. *Thermophysical Properties of Matter Volume 5: Spesific Heat Non Metallic Solid*; Plenum Publishing Corporation: New York, NY, USA, 1970.
34. Hidayat, M.I.P.; Fellicia, D.M.; Rafandi, F.I. Numerical simulation of temperature distribution in cylindrical ilmenite ($FeTiO_3$) due to microwave heating. In Proceedings of the 3rd International Conference on Materials and Metallurgical Engineering and Technology (Icommet 2017): Advancing Innovation in Materials Science, Technology and Applications for Sustainable Future, Surabaya, Indonesia, 30–31 October 2017; AIP Publishing: Melville, NY, USA, 2018; Volume 1945, p. 020018.
35. Oliveira, M.E.; Franca, A.S. Finite element analysis of microwave heating of solid products. *Int. Commun. Heat Mass Transf.* **2000**, *27*, 527–536. [CrossRef]